ORIGINAL ARTICLE

Mean field approximation of network of biophysical neurons driven by conductance-based ion exchange dynamics

Abhirup Bandyopadhyay[1] | **Spase Petkoski**[1] | **Viktor Jirsa**[1]

[1]Aix Marseille University, INSERM, Institute de Neuroscience des Systems, Marseille, France

Correspondence
Aix Marseille University, INSERM, Institute de Neuroscience des Systems, Marseille, 13005 France
Email: abhirup.BANDYOPADHYAY@univ-amu.fr

Funding information
Human Brain Project

Changes in extracellular ion concentrations are known to modulate neuronal excitability and play a major role in controlling the neuronal firing rate, not just during the healthy homeostasis, but also in pathological conditions such as epilepsy. The microscopic molecular mechanisms of field effects are understood, but the precise correspondence between the microscopic mechanisms of ion exchange in the cellular space of neurons and the macroscopic behavior of neuronal populations remains to be established. We derive a mean field model of a population of Hodgkin–Huxley type neurons. This model links the neuronal intra- and extracellular ion concentrations to the mean membrane potential and the mean synaptic input in terms of the synaptic conductance of the locally homogeneous mesoscopic network and can describe various brain activities including multistability at resting states, as well as more pathological spiking and bursting behaviors, and depolarizations. The results from the analytical solution of the mean field model agree with the mean behavior of numerical simulations of large-scale networks of neurons. The mean field model is analytically exact for non-autonomous ion concentration variables and provides a mean field approximation in the thermody-

namic limit, for locally homogeneous mesoscopic networks of biophysical neurons driven by an ion exchange mechanism. These results may provide the missing link between high-level neural mass approaches which are used in the brain network modeling and physiological parameters that drive the neuronal dynamics.

KEYWORDS
Hodgkin–Huxley type neurons, Mean field approximation, Lorentzian ansatz (LA), Resting state, Epilepsy

1 | INTRODUCTION

Different brain activities including perception, cognition, and several neurodegenerative disorders put forward the notion of understanding the brain dynamics as a large-scale complex system. Most of these activities can not be explained at the microscopic or single-cell level, rather they emerge through complex interactions between different regions of the brain with diverse neuronal activity. A common paradigm for studying the large-scale brain dynamics is through whole-brain network models [1], where regional populations interact through the white matter tracts. The local activity in this case is represented by neuronal mass models [2], which coupled together through the noise and the delays [3, 4] give rise to the emergent activity that can be linked to the neuroimaging signals [5]. The observable properties (variables) in the population level of a large-scale ensemble are generally explained by statistical physics formalism of mean-field theory which has been applied to neuronal dynamics to obtain several neural mass models to describe a range of local brain activities ([6], [7], [8], [9]). As such, these have shown to have individualized predictive value for resting state activity [10, 11], or for seizure generation and propagation in epilepsy [12], even if the latter was based on fully phenomenological model for the seizure onset and offset [13]. Regional heterogeneity improves the predictive value of whole-brain models in epilepsy, where it is informed by the clinical hypothesis [14], but also during data-driven fitting of the resting state [15]. The common roadblock here is that the used neuronal masses do not allow for direct expression of specific cytoarchitecural properties, which are becoming more available [16].

There is a significant gap in state of art literature in terms of the relationship between population-level behavior of the neuronal networks and the driving mechanism of neuronal dynamics that is the ion exchange at the cellular level. The mechanism of ion exchange in neuronal systems was first described by the famous Hodgkin–Huxley equations [17]. However, the assumption of constant intra- and extracellular ion concentrations in these equations became an issue for debate, especially in the mammalian brain. As a consequence, several studies investigated the role of the extracellular micro environment in pathological behaviors ([18]; [19]; [20]) as well as the cellular control of micro-environmental factors in modulating neuronal behavior ([19], [21]). Earlier studies ([19], [20], [21]) found that the reversal potentials of various ion species and their intra- and extracellular concentrations regulate the intrinsic excitability of neuronal networks. In the ion exchange mechanism of neuronal systems, the extracellular potassium concentration ($[K^+]_o$) and intracellular sodium concentration ($[Na^+]_i$) both change and are slowly balanced by the glia. In this process the increase in $[K^+]_o$ increases the potassium reversal potential and consequently the neuronal excitability, whereas the increase in $[Na^+]_i$ reduces the sodium reversal potential and the influx of sodium into the cell. These transient changes in $[K^+]_o$ are responsible for an overall fluctuation in excitability and spontaneous neuronal

activity ([22], [23], [21]).

The mammalian brain is a complex system comprising billions of neurons; thus, the computation of whole brain dynamics from the single neuron perspective exceeds the capacity of most modern super computers. Also, various brain imaging techniques measure the neuronal activities of brain regions to indicate the average activity of some neuronal ensembles. Since modeling the whole brain activity is impractical, developing a statistical physics based analytical framework of the population response (average behavior of large-scale neuronal ensembles) utilizing macroscopic or mesoscopic measures of network activity or mean field models for neuronal dynamics is essential. This approach has been experimentally validated in that different brain regions show similar responses to a given stimulus (for example different sensory regions of the cortex respond similarly to a given input) or to brain information processing and encoding, each of which requires coordinated activity and a high degree of redundancy among large ensembles of neurons. In this context, some phenomenological neuron models have been studied to understand the macroscopic dynamics of neuronal populations ([24]) or to provide statistical descriptions of neuronal networks ([6], [2], [25], [26]). In addition, several investigators addressed the macroscopic dynamics by using some statistical population measures, especially the firing rate, which measures the mean spike emission rate in a population ([27], [28], [1], [29], [13], [30], [5], [31], [32]). Some recent state-of-the-art studies also combined local neuronal dynamics with statistical descriptions in terms of the mean membrane potential and the firing rate in quadratic integrate-and-fire (QIF) neurons ([25], [33], [26]). Neural mass models and large scale brain dynamics models are also used for analyzing and identification of chaos in brain signal, epileptic seizure transmission, phase oscillation, evolution of network synchrony and several other problems ([34], [35], [36], [37], [38], [39], [40], [41], [42], [43]).

In spite of all these studies, as far as we are aware, no theory has linked macroscopically observable features of a large network of spiking neurons, with complex ion exchange dynamics. In this paper we approximated complex ion exchange dynamics by a step-wise QIF model by including two slow timescale biophysical variables. We demonstrated that the distribution of the neurons' membrane potentials could be described by a Lorentzian ansatz (LA). The continuity equation was solved to give rise to a mean field model with the same probability distribution of membrane potentials as the LA. The mean field model is exact for non-autonomous ion concentration variables and provides a mean field approximation within the thermodynamic limit, i.e., for a locally homogeneous mesoscopic network. Hence, we developed a mean field approximation for an all-to-all coupled network of heterogeneous neurons to approximately capture the behavior of ion exchange-driven neuronal dynamics. Moreover, considering some distributions of heterogeneous input current, we obtained a mean field approximation, described as a set of ordinary differential equations that fully described the macroscopic states of the recurrently connected spiking neurons.

2 | MATERIAL AND METHODS

The membrane potential of a single neuron in the brain is generally driven by an ion exchange mechanism in intracellular and extracellular space. The concentrations of potassium, sodium, and chlorine in the intracellular and extracellular space along with the active transport pump (Na^+/K^+ pump) in the cell membrane of neurons generate input currents to a neuron cell that drive the electrical behavior of a single neuron in terms of its membrane potential. The ion exchange mechanism in the cellular microenvironment, including local diffusion, glial buffering, ion pumps, and ion channels, has been mathematically modeled based on conductance-based ion dynamics to reflect the resting state and seizure behaviors in single neurons ([21], [44], [45]). The mechanism of ion exchange in the intracellular and extracellular space of the neuronal membrane is represented schematically in Figure 1. This biophysical interaction and ion exchange mechanism across the membrane of a neuron cell can be described as a Hodgkin–Huxley type dynamical

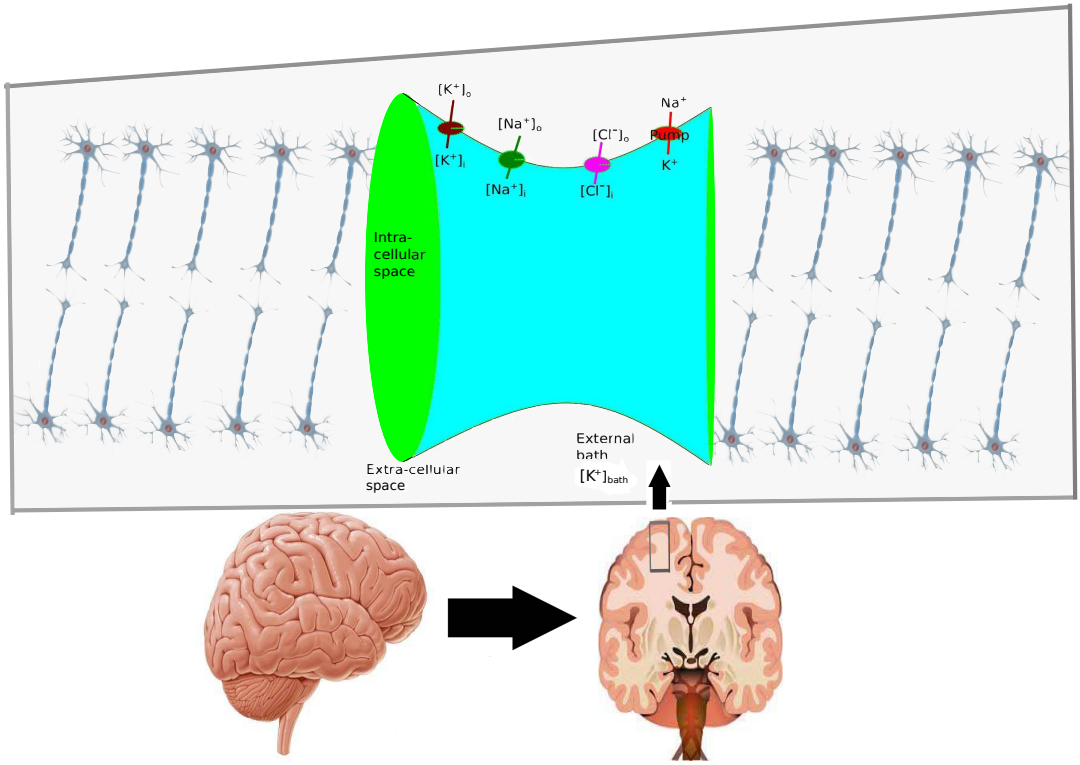

FIGURE 1 Schematic diagram of the ion channel mechanism in extracellular and intracellular space in the brain.

process, represented by the following dynamical system.

$$\begin{aligned}
\frac{dV}{dt} &= -\frac{1}{C_m}(J_{Cl} + J_{Na} + J_K + J_{pump}) \\
\frac{dn}{dt} &= \frac{n_\infty(V) - n}{\tau_n} \\
\frac{d\Delta[K^+]_i}{dt} &= -\frac{\gamma}{w_i}(J_k - 2J_{pump}) \\
\frac{d[K^+]_g}{dt} &= \epsilon([K^+]_{bath} + \beta\Delta[K^+]_i - \{[K^+]_{0,o} + [K^+]_g\})
\end{aligned} \tag{1}$$

This model represents the ion exchange mechanism of a single conductance-based neuron in terms of membrane potential (V), the potassium conductance gating variable (n), intracellular potassium concentration variation ($\Delta[K^+]_i$) and extracellular potassium buffering by the external bath ($[K^+]_g$). This mechanism considers ion exchange through the sodium, potassium, calcium-gated potassium, intracellular sodium, and extracellular potassium concentration gradients and leak currents. The intrinsic ionic currents of the neuron along with the sodium–potassium pump current and potassium diffusion regulate the concentrations of the different ion concentrations. The Nernst equation was used to couple the membrane potential of the neuron with the concentrations of the ionic currents. This mechanism gives rise to a slow-fast dynamical system in which the membrane potential (V) and potassium conductance gating variable (n) constitute the fast subsystem and the slow subsystem is represented in terms of the variation in the intracellular

potassium concentration ($\Delta[K^+]_i$) and extracellular potassium buffering by the external bath ($[K^+]_g$) (in (1)); where input currents due to different ionic substances and pump are represented as follows: ([21], [45]):

$$\begin{aligned} J_{Na} &= (g_{Na,l} + g_{Na} m_\infty(V) h(n))(V - 26.64 log(\frac{[Na^+]_o}{[Na^+]_i})) \\ J_K &= (g_{K,l} + g_K n)(V - 26.64 log(\frac{[K^+]_o}{[K^+]_i})) \\ J_{Cl} &= g_{Cl}(V + 26.64 log(\frac{[Cl^-]_o}{[Cl^-]_i})) \\ J_{pump} &= \rho \frac{1}{1 + exp(\frac{21 - [Na^+]_i}{2})} \frac{1}{1 + exp(5.5 - [K^+]_o)} \end{aligned} \tag{2}$$

The conductance functions are represented as follows:

$$\begin{aligned} n_\infty(V) &= \frac{1}{1 + exp(\frac{-19 - V}{18})} \\ m_\infty(V) &= \frac{1}{1 + exp(\frac{-24 - V}{12})} \\ h(n) &= 1.1 - \frac{1}{1 + exp(-8(n - 0.4))} \end{aligned} \tag{3}$$

In this model the concentration of chloride ion is invariant and the extracellular and intracellular concentrations of potassium, sodium, and chlorine ions are represented in terms of these state variables as follows:

$$\begin{aligned} \Delta[Na^+]_i &= -\Delta[K^+]_i \\ \Delta[Na^+]_o &= -\beta \Delta[Na^+]_i \\ \Delta[K^+]_o &= -\beta \Delta[K^+]_i \\ [Na^+]_i &= [Na^+]_{0,i} + \Delta[Na^+]_i \\ [Na^+]_o &= [Na^+]_{0,o} + \Delta[Na^+]_o \\ [K^+]_o &= [K^+]_{0,o} + \Delta[K^+]_o + [K]_g \\ [Cl^-]_o &= [Cl^-]_{0,o}, [Cl^-]_i = [Cl^-]_{0,i} \end{aligned} \tag{4}$$

The biophysically relevant values of the parameters could be obtained from several previous studies and from in vivo and in vitro experiments ([21], [45]). Those that we used for the simulation are shown in Table-1.

3 | MEAN FIELD APPROXIMATION OF COUPLED NEURONS

The next aim was to develop a mean field model for a heterogeneous population of the all-to-all coupled biophysical neurons described by (1) within the thermodynamic limit, i.e., when the number of neurons $N \to \infty$. To consider the impact of other spiking neurons in a network on a single neuron through the synaptic input current, first the synaptic kinetics needed to be modeled. The basic mechanism of synaptic transmission can be described as the mechanism by which a neurotransmitter is released into the synaptic cleft as a result of an influx of calcium through presynaptic calcium channels as the presynaptic pulse (spike) depolarizes the synaptic terminal. The neurotransmitter plays a crucial role in opening the postsynaptic channels, which causes the flow of the ionic current across the membrane. This

Parameters	symbols	values
Membrane capacitance	C_m	1nF
Gating time constant	τ_n	$4S^{-1}$
Chloride conductance	g_{Cl}	7.5nS
Maximal potassium conductance	g_K	22nS
Maximal sodium conductance	g_{Na}	40nS
Potassium leak conductance	$g_{K,l}$	0.12nS
Sodium leak conductance	$g_{Na,l}$	0.02nS
Intracellular volume	ω_i	2160μ m
Extracellular volume	ω_o	720μ m
Intra/extra cellular volume ratio	$\beta = \frac{\omega_i}{\omega_o}$	3
Concentration changes time constant	γ	$0.04S^{-1}$
Diffusion time constant	ϵ	$0.001S^{-1}$
Maximal Na/K pump current	ρ	250pA
External bath of K	$[K^+]_{bath}$	8mM
Initial concentration of Extracellular K	$[K^+]_{0,o}$	4.8 mM
Initial concentration of Intracellular K	$[K^+]_{0,i}$	130 mM
Initial concentration of Extracellular Na	$[Na^+]_{0,o}$	138 mM
Initial concentration of Intracellular Na	$[Na^+]_{0,i}$	16 mM
concentration of Extracellular Cl	$[Cl^-]_{0,o}$	112 mM
concentration of Intracellular Cl	$[Cl^-]_{0,i}$	5 mM

TABLE 1 List of parameters and their values used for the simulation

mechanism is often represented by phenomenological models, which assume that the normalized synaptic conductance $g_{syn}(t)$ from 0 to 1 rises instantaneously at the time of the kth pulse (spike), t^k and consequently undergoes an exponential decay with some rate constant τ. This mechanism is traditionally modeled by the following differential equation

$$\tau \frac{dg_{syn}(t)}{dt} = \sum_{j=1}^{N} [-g_{syn}(t) + \delta(t_j^k - t)(1 - g_{syn}(t))] \tag{5}$$

The solution can be written as $g_{syn}(t) = \sum_{j=1}^{N} [\frac{t-t_j^k}{\tau} e^{\frac{t-t_j^k}{\tau}}]$ ([46], [47]). Here, $\delta(t)$ is the Dirac delta function, and t_j^k represents the time of the kth pulse (spike) of the jth neuron. Then, the synaptic input current is given as follows:

$$I_{syn} = k g_{syn}(t)(V - E) \tag{6}$$

where V is the postsynaptic potential; E is the potential, termed the synaptic reversal potential, at which the direction of the net current flow reverses; and represents the maximum conductance of the synapse. At this point we approximated the four-dimensional dynamics in 1 to a three-dimensional system in order to represent the fast subsystem in terms of membrane potential alone. This allowed us to represent the probability distribution of V in terms of a single fast variable V and to use consequent mathematical formalism to solve the mean field behavior of the large network of neurons. This was done by eliminating the second fast variable from the system by averaging $\frac{dV}{dt}$ over n, i.e., replacing $\frac{dV}{dt} = f(V, n, \Delta[K^+]_i, [K^+]_g)$ with $\frac{dV}{dt} = \frac{1}{\limsup n - \liminf n}\int_{\liminf n}^{\limsup n} f(V, n, \Delta[K^+]_i, [K^+]_g)dn$, where $f(V, n, \Delta[K^+]_i, [K^+]_g)$ represents the right-hand side of the V dynamics in 1. We modeled the average of n as

$$\langle n \rangle = \begin{Bmatrix} n_\infty(V), \Delta[K^+]_i > \alpha \\ 2.0 + 0.02\langle V \rangle, \Delta[K^+]_i \leq \alpha \end{Bmatrix}$$

where $\alpha = k_\alpha + \mu_1([K^+]_{bath} - k_0) + \mu_2([K^+]_{bath} - k_0)^2$ with $k_\alpha = -0.8825, \mu_1 = -0.3965, \mu_2 = 0.0075, k_0 = 11.5$. Applying this averaging method and substituting $\langle n \rangle$ into the current terms

$$\begin{aligned} I_{Na} &= (g_{Na,l} + g_{Na} m_\infty(V) h(\langle n \rangle))(V - 26.64 log(\frac{[Na^+]_o}{[Na^+]_i})) \\ I_K &= (g_{K,l} + g_K \langle n \rangle)(V - 26.64 log(\frac{[K^+]_o}{[K^+]_i})) \\ I_{Cl} &= J_{Cl} = g_{Cl}(V + 26.64 log(\frac{[Cl^-]_o}{[Cl^-]_i})) \\ I_{pump} = J_{pump} &= \rho \frac{1}{1 + exp(\frac{21 - [Na^+]_i}{2})} \frac{1}{1 + exp(5.5 - [K^+]_o)} \end{aligned}$$

we obtained the 3-dimensional averaged dynamical model for 1 as follows

$$\begin{aligned} \frac{dV}{dt} &= -\frac{1}{C_m}(I_{Cl} + I_{Na} + I_K + I_{pump}) \\ \frac{d\Delta[K^+]_i}{dt} &= -\frac{\gamma}{w_i}(I_k - 2I_{pump}) \\ \frac{d[K^+]_g}{dt} &= \epsilon([K^+]_{bath} + \beta\Delta[K^+]_i - \{[K^+]_{0,o} + [K^+]_g\}) \end{aligned} \tag{7}$$

Hence, we obtained the system of the following set of ordinary differential equations to describe the microscopic population state of the ion exchange driven network of biophysical neurons:

$$\begin{aligned} \frac{dV}{dt} &= -\frac{1}{C_m}(I_{Cl} + I_{Na} + I_K + I_{pump}) + Jg_{syn}(t)(V_j - E_j) + \eta_j \\ \frac{d\Delta[K^+]_i}{dt} &= -\frac{\gamma}{w_i}(I_k - 2I_{pump}) \qquad ; j = 1, 2, ..., N \\ \frac{d[K^+]_g}{dt} &= \epsilon([K^+]_{bath} + \beta\Delta[K^+]_i - \{[K^+]_{0,o} + [K^+]_g\}) \end{aligned} \tag{8}$$

where J is the global coupling coefficient, η_j is the heterogeneous quenched external input, and E_j is the synaptic reversal potential of jth neuron. For the thermodynamic limit $N \to \infty$, (8) has the following form

$$\begin{aligned} \frac{dV}{dt} &= -\frac{1}{C_m}(I_{Cl} + I_{Na} + I_K + I_{pump}) + Jg_{syn}(t)(V - E) + \eta \\ \frac{d\Delta[K^+]_i}{dt} &= -\frac{\gamma}{w_i}(I_k - 2I_{pump}) \\ \frac{d[K^+]_g}{dt} &= \epsilon([K^+]_{bath} + \beta\Delta[K^+]_i - \{[K^+]_{0,o} + [K^+]_g\}) \end{aligned} \tag{9}$$

The $\frac{dV}{dt}$ equation in (9) is modeled as a step wise quadratic function based on the nullcline geometry of the microscopic state of the membrane potential V and the dynamics of the biophysical population of neurons $\{V_j\} : j = 1, 2, ..., N$ is hence represented as the following step wise quadratic function of $\{V_j\}$.

$$\frac{dV_j}{dt} = \begin{Bmatrix} b_1\{(V_j - d_{1,j})^2 + I_{1,j} + Jg_{syn}(t)(V_j - E_j)\}; \forall V_j \geq s \\ b_2\{(V_j - d_{2,j})^2 + I_{2,j} + Jg_{syn}(t)(V_j - E_j)\}; \forall V_j < s \end{Bmatrix}$$

For a homogeneous population within the thermodynamic limit $N \to \infty$ this can be represented by removing the index as follows:

$$\frac{dV}{dt} = \begin{Bmatrix} b_1\{(V - d_1)^2 + I_1 + Jg_{syn}(t)(V - E)\}; \forall V \geq s \\ b_2\{(V - d_2)^2 + I_2 + Jg_{syn}(t)(V - E)\}; \forall V < s \end{Bmatrix} \tag{10}$$

Here the terms I_1 and I_2 are functions of $\Delta[K^+]_i$ and $[K^+]_{bath}$ but are independent of V and are given as follows:

$$I_1 = \frac{\psi_1}{b_1}(\Delta[K^+]_i - k_0) + \frac{a_1}{b_1} + \eta, I_2 = \frac{\psi_2}{b_2}(\Delta[K^+]_i - k_0) + \frac{a_2}{b_2} + \eta \tag{11}$$

Here d_1, d_2 and a_2 are functions of $[K^+]_{bath}$ and a_1 which, in turn, is function of $\Delta[K^+]_i$ and $[K^+]_{bath}$. The parameters b_1, b_2, and s, are constants estimated from the nullclines geometry of system (1) as follows:
$d_1 = q_1 + r_{11}([K^+]_{bath} - k_0) + +r_{12}([K^+]_{bath} - k_0)^2, d_2 = q_2 + r_{21}([K^+]_{bath} - k_0) + r_{22}([K^+]_{bath} - k_0)^2,$
$a_2 = q_3 + \lambda_1([K^+]_{bath} - k_0) + \lambda_2([K^+]_{bath} - k_0)^2, a_1 = a_2 + (\psi_2 - \psi_1)(\Delta[K^+]_i - k_0) - b_1(s - d_1)^2 + b_2(s - d_2)^2$ with the parameter values $s = -37, b_1 = -0.50, b_2 = 0.11, k_0 = 11.5, r_{11} = 0.45, r_{12} = -0.50, r_{21} = 2.5, r_{22} = -0.1, \lambda_1 = 30.0, \lambda_2 = -0.05, q_1 = -25.2, q_2 = -56.0, q_3 = -72.5, \psi_1 = 50.0, \psi_2 = 112.5$. The validity of the fit of these parameters is shown in Figure 2.

Also, η in the (11) refers to the heterogeneous quenched component, which represents the heterogeneity in the network of neurons and is distributed according to some probability distribution, say $g(\eta)$. For the mean field approximation in the thermodynamic limit $N \to \infty$, let us denote $\rho(V, \Delta[K^+]_i, [K^+]_{bath}, \eta, t)dV$ as the fraction of neurons with a membrane potential between V and $V + dV$ where η is the random variable heterogeneity parameter (heterogeneous input current), which could be considered to be distributed according to the probability distribution $g(\eta)$. Then, the total voltage density can be written as $\int_{-\infty}^{\infty} \rho(V, \Delta[K^+]_i, [K^+]_{bath}, \eta, t)g(\eta)d\eta$. This setup leads to the continuity equation

$$\delta_t \rho + \delta_V[\frac{dV}{dt}\rho] = 0 \tag{12}$$

It should be noted here that the approximation of (1) by (7) by removing n from the system through the averaging

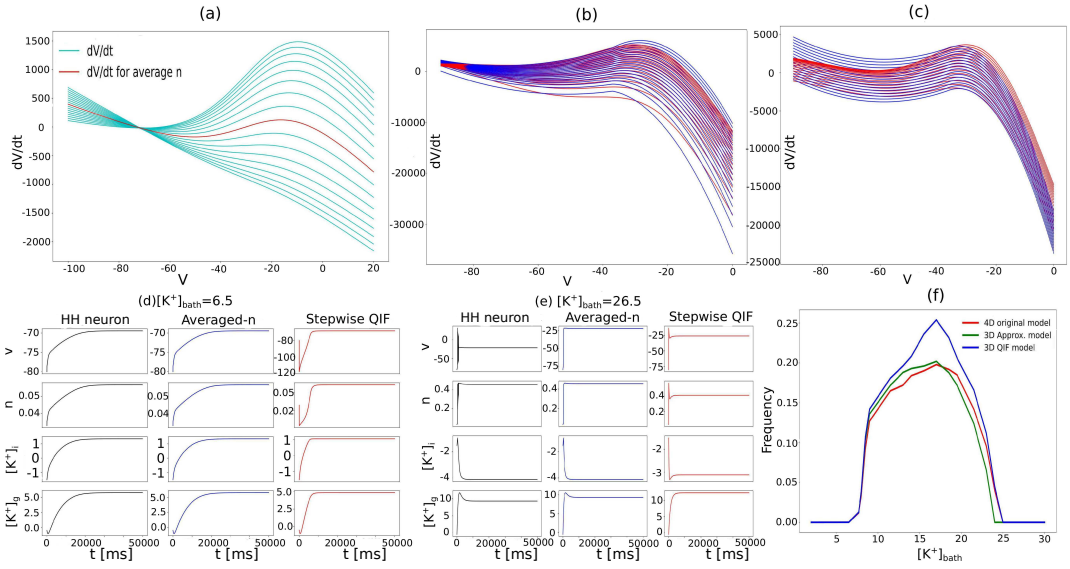

FIGURE 2 Dependence of $\frac{dV}{dt}$ [mV] on n: (a) $\frac{dV}{dt}$ [mV] for different values of n in cyan and the average trajectory in red. (b) Approximation of $\frac{dV}{dt}$ [mV] for different values of $\Delta[K^+]_i$ $[mol\backslash m^3]$: original functions in red and approximations in blue. (c) Approximation of $\frac{dV}{dt}$ [mV] for different values of $[K^+]_{bath}$ $[mol\backslash m^3]$: original functions in red and approximations in blue. (d-e) Simulation of the dynamics: time series of V [mV] (in red), n (in blue), $\Delta[K^+]_i$ $[mol\backslash m^3]$ (in green), and $[K]_g$ $[mol\backslash m^3]$ (in black): from the left original 4D system (1st column), 3D approximation (2nd column), 3D stepwise QIF approximation (3rd column); for (d) $[K^+]_{bath} = 6.5$, (e) $[K^+]_{bath} = 26.5$. (f) Frequency of oscillation: for the original 4D model in red; for the reduced 3D model in green; for the stepwise QIF approximation in blue.

method is an intermediate approximation, which ensures the integrability of the ρ and allowed us to solve the continuity (12). However, we reused the functional forms in the mean field equation as in (1) and continued this through the solution of the continuity equation. This resulted in retaining the original dynamic behavior of the system, and the intermediate approximation allowed us to derive the mean field equation analytically. At this point adiabatic reduction was applied to the slow variables, and the differential equation representing the V dynamics along with the coupling term was considered to be involved with only the V, η, and t variables. This reduced the V dynamics ($\frac{dV}{dt}$ equation) in (9) to a function of V and t only for each value of η. Consequently, we could consider ρ as a function of only V, η, and t (as similar methodologies were applied in different literature like [48], [49]). Therefore, we denoted the right-hand side of the V dynamics as a function $f(t, V, \eta)$ and represent it as follows:

$\frac{dV}{dt} = -\frac{1}{C_m}(I_{Cl} + I_{Na} + I_K + I_{pump}) + Jg_{syn}(t)(V - E) + \eta = f(t, V, \eta)$

That reduces (12) to $\frac{\delta\rho}{\delta t} + f(t, V)\frac{\delta\rho}{\delta V} = -f_V(t, V)\rho$ which is a first order quasi-linear PDE, could be solved by the Lagrange method using the Lagrange subsidiary equation

$$\frac{dt}{1} = \frac{dV}{f(t, V)} = \frac{d\rho}{-f_V(t, V)\rho} \tag{13}$$

where $f_V(t, V)$ represents the derivative of f with respect to V. Integrating from last two ratios we got an independent solution in which ρ is proportional to $\frac{1}{f(t,V)}$, i.e., $\rho \propto \frac{1}{f(t,V)}$. Hence, the trivial solution of the continuity equation (12) has the functional form $\rho_0(V, \Delta[K^+]_i, [K^+]_{bath}, \eta, t) \propto (\frac{dV}{dt})^{-1}$ that is inversely proportional to their time derivative

for each value of η.

$$\rho(V, \Delta[K^+]_i, [K^+]_{bath}, \eta, t) = \left\{ \begin{array}{l} \frac{K_1}{b_1\{(V-d_1)^2+I_1\}}; \forall V \geq s \\ \frac{K_2}{b_2\{(V-d_2)^2+I_2\}}; \forall V < s \end{array} \right\} \tag{14}$$

Here k_1 and k_2 are constants, so that the integral becomes one. Since I_1, I_2, d_1 and d_2 are functions of $[K^+]_{bath}$ and $\Delta[K^+]_i$ within the thermodynamic limit $N \to \infty$, the differential equation for the membrane potential can be represented as

$$\frac{dV}{dt} = \left\{ \begin{array}{l} b_1\{[V - y(\eta, \Delta[K^+]_i, [K^+]_{bath}, t)]^2 + [x(\eta, \Delta[K^+]_i, [K^+]_{bath}, t)]^2\}; \forall V \geq s \\ b_2\{[V - y(\eta, \Delta[K^+]_i, [K^+]_{bath}, t)]^2 + [x(\eta, \Delta[K^+]_i, [K^+]_{bath}, t)]^2\}; \forall V < s \end{array} \right\} \tag{15}$$

And the probability density function ρ can be written as

$$\rho(V, \Delta[K^+]_i, [K^+]_{bath}, \eta, t) = \left\{ \begin{array}{l} \frac{K_1}{b_1\{[V-y(\eta,\Delta[K^+]_i,[K^+]_{bath},t)]^2+[x(\eta,\Delta[K^+]_i,[K^+]_{bath},t)]^2\}}; \forall V \geq s \\ \frac{K_2}{b_2\{[V-y(\eta,\Delta[K^+]_i,[K^+]_{bath},t)]^2+[x(\eta,\Delta[K^+]_i,[K^+]_{bath},t)]^2\}}; \forall V < s \end{array} \right\} \tag{16}$$

Since for each values of η , $\int_{-\infty}^{\infty} \rho dV = 1$, we found solutions for constants $k_1 = \frac{b_1 x}{\pi}$ and $k_2 = \frac{b_2 x}{\pi}$ which reduces the relevant dynamics to a lower dimensional space and the solution of (12) converges to some Lorentzian type function independently of the initial condition. Then, the corresponding conditional probability can be expressed as a Lorentzian ansatz (LA) ([25], [26]), as follows:

$$\rho(V, \Delta[K^+]_i, [K^+]_{bath}, \eta, t) = \frac{1}{\pi} \frac{x(\eta, \Delta[K^+]_i, [K^+]_{bath}, t)}{[V - y(\eta, \Delta[K^+]_i, [K^+]_{bath}, t)]^2 + [x(\eta, \Delta[K^+]_i, [K^+]_{bath}, t)]^2} \tag{17}$$

Here, $y(\eta, \Delta[K^+]_i, [K^+]_{bath}, t)$ is related to the mean membrane potential of each value of η. $\langle V(\eta, \Delta[K^+]_i, [K^+]_{bath}, t)\rangle = \int_{-\infty}^{\infty} \rho(V, \eta, \Delta[K^+]_i, [K^+]_{bath}, t) V dV = v(\eta, \Delta[K^+]_i, [K^+]_{bath}, t)$, (say)
$= \int_{-\infty}^{\infty} \frac{1}{\pi} \frac{x(\eta,\Delta[K^+]_i,[K^+]_{bath},t)}{[V-y(\eta,\Delta[K^+]_i,[K^+]_{bath},t)]^2+[x(\eta,\Delta[K^+]_i,[K^+]_{bath},t)]^2} V dV = \frac{x}{\pi} \int_{-\infty}^{\infty} \frac{V-y+y}{(V-y)^2+x^2} dV = \frac{x}{\pi} \int_{-\infty}^{\infty} [\frac{V-y}{(V-y)^2+x^2} dV + \frac{y}{(V-y)^2+x^2} dV] =$
$\frac{x}{\pi} \lim_{R\to\infty} [\frac{1}{2} log(\frac{[R-y]^2+x^2}{[-R-y]^2+x^2}) + \frac{y}{x}[tan^{-1}(R) - tan^{-1}(-R)]]$
i.e., $v(\eta, \Delta[K^+]_i, [K^+]_{bath}, t) = y(\eta, \Delta[K^+]_i, [K^+]_{bath}, t)$ [taking the P.V. of the Cauchy integral] and

$$v(t) = \int_{-\infty}^{\infty} y(\eta, \Delta[K^+]_i, [K^+]_{bath}, t) g(\eta) d\eta \tag{18}$$

Now, we solved the continuity equation (12) with LA ((17))

$$\delta_t \rho = \frac{1}{\pi} \frac{[(V-y)^2 + x^2]\dot{x} - x[-2(V-y) + 2x\dot{x}]}{[(V-y)^2 + x^2]^2} = \frac{1}{\pi} \frac{\dot{x}V^2 - 2(y\dot{x} + x\dot{y})V + ([y^2 - x^2]\dot{x} - 2xy\dot{y})}{[(V-y)^2 + x^2]^2} \tag{19}$$

Here overdot represents the derivative with respect to time. We took the rate of change of the membrane potential as (10) and obtained

$$\delta_V(\dot{V}\rho) = \ddot{V}\rho + \dot{V}\delta_V(\rho) = \left\{ \begin{array}{l} \frac{1}{\pi} \frac{(2b_1(V-d_1 J g_{syn})x}{[(V-y)^2+x^2]} - \frac{2x\dot{V}(V-y)}{\pi[(V-y)^2+x^2]^2}; \forall V \geq s \\ \frac{1}{\pi} \frac{(2b_2(V-d_2 J g_{syn})x}{[(V-y)^2+x^2]} - \frac{2x\dot{V}(V-y)}{\pi[(V-y)^2+x^2]^2}; \forall V < s \end{array} \right\} =$

$$\frac{[2b_1d_1x-2b_1xy-Jg_{syn}x]V^2+2[b_1x^3+b_1xy^2-b_1d_1^2x-b_1I_1x+Jg_{syn}Ex]V+[(Jg_{syn}-2b_1d_1)(x^2+y^2)x+2(b_1d_1^2+b_1I_1-Jg_{syn}E)xy+(y^2-x^2)\dot{x}-2xy\dot{y}]}{\pi[(V-y)^2+x^2]^2}$$
$$\frac{[2b_2d_2x-2b_2xy-Jg_{syn}x]V^2+2[b_2x^3+b_2xy^2-b_2d_2^2x-b_2I_2x+Jg_{syn}Ex]V+[(Jg_{syn}-2b_2d_2)(x^2+y^2)x+2(b_2d_2^2+b_2I_2-Jg_{syn}E)xy+(y^2-x^2)\dot{x}-2xy\dot{y}]}{\pi[(V-y)^2+x^2]^2}$$

Hence, equating continuity equation (12) for being an identity, that is only if all the coefficients of the powers of V are zero, we get (from the coefficient of $V^2 = 0$)

$$\dot{x} = \begin{Bmatrix} [2b_1(y-d_1)+Jg_{syn}]x; \forall V \geq s \\ [2b_2(y-d_2)+Jg_{syn}]x; \forall V < s \end{Bmatrix} \tag{20}$$

From the coefficient of $V = 0$ we get

$$\begin{Bmatrix} b_1x^3+b_1xy^2-b_1d_1^2x-b_1I_1x+Jg_{syn}Ex-y\dot{x}+x\dot{y}=0; \forall V \geq s \\ b_2x^3+b_2xy^2-b_2d_2^2x-b_2I_2x+Jg_{syn}Ex-y\dot{x}+x\dot{y}=0; \forall V < s \end{Bmatrix}$$

$$\Rightarrow \dot{y} = \begin{Bmatrix} b_1[(y-d_1)^2+I_1-x^2]+Jg_{syn}(y-E); \forall V \geq s \\ b_2[(y-d_2)^2+I_2-x^2]+Jg_{syn}(y-E); \forall V < s \end{Bmatrix} \tag{21}$$

This leads to the constant term to be zero and we obtained the mean field model, as follows:

$$\begin{Bmatrix} \dot{x} = [2b_1(y-d_1)+Jg_{syn}]x, \dot{y} = b_1[(y-d_1)^2+I_1-x^2]+Jg_{syn}(y-E); \forall V \geq s \\ \dot{x} = [2b_2(y-d_2)+Jg_{syn}]x, \dot{y} = b_2[(y-d_2)^2+I_2-x^2]+Jg_{syn}(y-E); \forall V < s \end{Bmatrix}$$

This pair of equations can be represented by a single complex valued equation, as follows:

$$\delta_t\omega(\eta,\Delta[K^+]_i,[K^+]_{bath},t) = \begin{Bmatrix} ib_1[(i\omega+d_1)^2+I_1]+Jg_{syn}[i\omega+2y-E]; \forall V \geq s \\ ib_2[(i\omega+d_2)^2+I_2]+Jg_{syn}[i\omega+2y-E]; \forall V < s \end{Bmatrix} \tag{22}$$

where $\omega(\eta,\Delta[K^+]_i,[K^+]_{bath},t) = x(\eta,\Delta[K^+]_i,[K^+]_{bath},t)+iy(\eta,\Delta[K^+]_i,[K^+]_{bath},t)$ and real and complex components of (22) represent the dynamics of y and x respectively.

Moreover, if we consider the distribution of the heterogeneous input current η to be a Lorentzian distribution with half-width Δ and location of the center be $\overline{\eta}$, i.e. :

$$g(\eta) = \frac{1}{\pi}\frac{\Delta}{(\eta-\overline{\eta})^2-\Delta^2} \tag{23}$$

Then, the residue theorem can be applied to compute the integral in (18) over the closed contour in the complex η-plane. It should be noted that the assumption of $g(\eta)$ as a Lorentzian distribution leads to the conclusion that $v(t)$ and $x(t)$ could be computed by Cauchy residue theorem with the value of ω at $\eta = \overline{\eta}-i\Delta$, i.e., at the pole of the Lorentzian distribution (23) in the lower half of η-plane: $x(\Delta[K^+]_i,[K^+]_{bath},t)+iy(\Delta[K^+]_i,[K^+]_{bath},t) = \omega(\overline{\eta}-i\Delta,\Delta[K^+]_i,[K^+]_{bath},t)$. Thus evaluating (23) at $\eta = \overline{\eta}-i\Delta$ we obtained the mean field model of membrane potential in terms of two coupled differential equations, as follows:

$$\begin{Bmatrix} \dot{x} = b_1(\Delta+2x(v-d_1))+Jg_{syn}x, \dot{v} = b_1[(v-d_1)^2+\overline{\eta}+I_1-x^2]+Jg_{syn}(v-E); \forall v \geq s \\ \dot{x} = b_2(\Delta+2x(v-d_2))+Jg_{syn}x, \dot{v} = b_2[(v-d_2)^2+\overline{\eta}+I_2-x^2]+Jg_{syn}(v-E); \forall v < s \end{Bmatrix}$$

Hence, the 4-dimensional mean field equation with $\Delta[K^+]_i$ becomes the following:

$$\begin{aligned}
\frac{dx}{dt} &= \begin{Bmatrix} [b_1(\Delta + 2x(v-d_1)) + Jg_{syn}x; \forall V \geq s \\ [b_2(\Delta + 2x(v-d_2)) + Jg_{syn}x; \forall V < s \end{Bmatrix} \\
\frac{dv}{dt} &= \begin{Bmatrix} b_1[(v-d_1)^2 + \overline{\eta} + I_1 - x^2] + Jg_{syn}(v-E); \forall V \geq s \\ b_2[(v-d_2)^2 + \overline{\eta} + I_2 - x^2] + Jg_{syn}(v-E); \forall V < s \end{Bmatrix} \\
\frac{d\Delta[K^+]_i}{dt} &= -\frac{\gamma}{w_i}(I_k(v) - 2I_{pump}) \\
\frac{d[K^+]_g}{dt} &= \epsilon([K^+]_{bath} + \beta\Delta[K^+]_i - \{[K^+]_{0,o} + [K^+]_g\})
\end{aligned} \tag{24}$$

Here v denotes the mean membrane potential, x is a phenomenological variable, and intracellular potassium concentration variation and extracellular potassium buffering by the external bath are denoted by $\Delta[K^+]_i$ and $[K]_g$ respectively. It should be noted that here the phenomenological variable x and its dynamics only depend upon v by construction. So, technically, the dynamical system in (24) could be characterized by only one fast variable v. Consequently, with only one fast variable the dynamics cannot demonstrate fast oscillations but only the envelope of the oscillations, as demonstrated in Figure 3. Therefore, the spike train and tonic spike features in the corresponding regime of the dynamics, which are characterized by sharp oscillations in the v and n dimensions alone, are lost through averaging out n from the system (1).

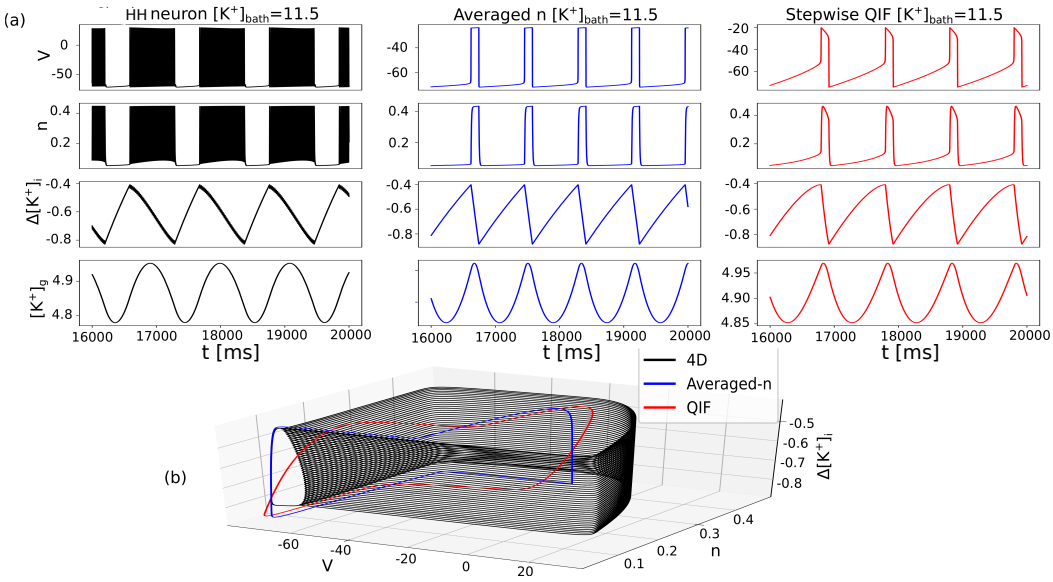

FIGURE 3 Simulation of the dynamics: (a) Time series of V [mV] (1st row), n (2nd row), $\Delta[K^+]_i$ $[mol\backslash m^3]$ (3rd row), and $[K]_g$ $[mol\backslash m^3]$ (4th row): from the left original 4D system (in black), 3D approximation (in blue), 3D stepwise QIF approximation (in red); (b) 3D Phase space with V [mV], n, and $\Delta[K^+]_i$ $[mol\backslash m^3]$ for three models with the original 4D model in black, for the reduced 3D model in blue, and for the stepwise QIF approximation in red; for $[K^+]_{bath} = 11.5$.

Moreover, the variable n represents the probability of channel opening, and in principle, the expected probability

of channel opening is proportional to the synaptic conductance. Therefore, at this point we defined the normalized synaptic conductance g_{syn} as cn within the thermodynamic limit. This also allowed us to replace the step-wise QIF approximation by the original functional forms in the mean field model, as (10) is an approximation of (9) in the first place. Here we can replace the step-wise quadratic functions in (10) by the original function from (9), including the synaptic conductance variable n. Hence, the final mean field approximation is a five-dimensional dynamical system as follows:

$$\begin{aligned}
\frac{dx}{dt} &= \begin{Bmatrix} b_1(\Delta + 2x(v-d_1)) + cJnx; \forall V \geq s \\ b_2(\Delta + 2x(v-d_2)) + cJnx; \forall V < s \end{Bmatrix} \\
\frac{dv}{dt} &= \begin{Bmatrix} -\frac{1}{C_m}(J_{Cl} + J_{Na} + J_K + J_{pump}) - b_1 x^2 + \overline{\eta} + cJn(v-E); \forall V \geq s \\ -\frac{1}{C_m}(J_{Cl} + J_{Na} + J_K + J_{pump}) - b_2 x^2 + \overline{\eta} + cJn(v-E); \forall V < s \end{Bmatrix} \\
\frac{dn}{dt} &= \frac{(\frac{1}{1+exp(\frac{-19-V}{18})}) - n}{\tau_n} \\
\frac{d\Delta[K^+]_i}{dt} &= -\frac{\gamma}{w_i}(I_k(v) - 2I_{pump}) \\
\frac{d[K^+]_g}{dt} &= \epsilon([K^+]_{bath} + \beta\Delta[K^+]_i - \{[K^+]_{0,o} + [K^+]_g\})
\end{aligned} \tag{25}$$

If we consider the inhibitory and excitatory group of neurons, the corresponding mean field approximation can be written as follows:

$$\begin{aligned}
\frac{dx}{dt} &= \begin{Bmatrix} b_1(\Delta + 2x(v-d_1)) + (c_i + c_e)Jnx; \forall V \geq s \\ b_2(\Delta + 2x(v-d_2)) + (c_i + c_e)Jnx; \forall V < s \end{Bmatrix} \\
\frac{dv}{dt} &= \begin{Bmatrix} -\frac{1}{C_m}(J_{Cl} + J_{Na} + J_K + J_{pump}) - b_1 x^2 + \overline{\eta} + c_i Jn(v-E_i) + c_e Jn(v-E_e); \forall V \geq s \\ -\frac{1}{C_m}(J_{Cl} + J_{Na} + J_K + J_{pump}) - b_2 x^2 + \overline{\eta} + c_i Jn(v-E_i) + c_e Jn(v-E_e); \forall V < s \end{Bmatrix} \\
\frac{dn}{dt} &= \frac{(\frac{1}{1+exp(\frac{-19-V}{18})}) - n}{\tau_n} \\
\frac{d\Delta[K^+]_i}{dt} &= -\frac{\gamma}{w_i}(I_k(v) - 2I_{pump}) \\
\frac{d[K^+]_g}{dt} &= \epsilon([K^+]_{bath} + \beta\Delta[K^+]_i - \{[K^+]_{0,o} + [K^+]_g\})
\end{aligned} \tag{26}$$

Where E_e and E_i are the synaptic reversal potentials of the excitatory and inhibitory groups of neurons.

4 | RESULT AND DISCUSSION

In this paper we have derived a mean-field approximation of locally homogeneous network of Hodgkin–Huxley type neurons (HH neuron) with heterogeneous quenched external input η (25, and 26). The appropriateness of mean-field approximation is validated by comparing the simulation results of the large network of coupled HH neurons with the mean-field model (26) which appears to be quite robust under stochasticity and different type of distribution of heterogeneous quenched external input η (Figure-4). Our model demonstrates different types of spiking and bursting behavior as well as resting-state (Figure-6) and multistability in the distinct regime of external potassium bath ($[K^+]_{bath}$). These kinds of neuronal activities are quite observable in large-scale brain dynamics which by the means

of this novel mean-field model get connected with the ion exchange mechanism and the ion concentration states in the cellular space. The bifurcation analysis of the mean-field model is carried out to identify relevant parameter regime which is responsible for different types of spiking and bursting behavior, resting-state, and multistability features in the mean-field model (Figure-5). Furthermore, it is observed that even if in the resting state (healthy) network certain kinds of external stimulus current could generate transient neuronal bursts (in terms of transition between upstate and downstate) which are validated by co-simulation of the large network of coupled HH neurons and the mean-field model (Figure-7). This result could be quite significant in terms of explaining the neuronal activities during brain stimulation.

The simulation of Hodgkin–Huxley type single neuron dynamics (1) driven by an ion exchange mechanism, has revealed that the parameter $[K^+]_{bath}$ is the most important parameter for describing the dynamics. Previous studies showed that changing the value of the concentration of the external potassium bath is responsible for qualitative changes in the dynamical behavior of a single neuronal system [45], particularly discovering that in the parameter regime $[K^+]_{bath} = [6.01, 6.875]$ multistability occurs.

Reproducing the bifurcation analysis by a numerical continuation revealed two stable fixed points and a stable focus in this regime for $[K^+]_{bath}$. We also observed a Hopf bifurcation at $[K^+]_{bath} = 7.68$. At higher values of $[K^+]_{bath}$ he stable fixed-point behavior of the dynamics changes into limit cycle behavior and the dynamics shows the bursting characteristics of neurons. The single neuron model was also shown to be able to produce different dynamic behaviors of single neuronal activity, such as epileptic bursts, status epilepticus, resting state, etc. In this study we developed a mean-field dynamics system based on a biophysical single neuron model (1) to describe the network behavior of biophysical neurons within the thermodynamic limit.

To be able to apply convenient mathematical (analytical) methods in this study, the velocity of the membrane potential of a single neuron described by (1) was approximated as a stepwise quadratic function because geometrically it resembles a combination of two inverted parabolas. The validity of this approximation is shown in Figure 2 where the time derivative of V in (1) is compared with that of a stepwise quadratic approximation. The appropriateness of the approximation of the membrane potential dynamics is represented for different values of the other state variables and parameters, such as n, $\Delta[K^+]_i$, and $[K^+]_{bath}$ in Figures 2(a), 2(b), and 2(c), respectively.

The approximation of the membrane potential dynamics as a stepwise quadratic function allowed us to apply analytical approaches and to solve the corresponding continuity equation to derive the mean field of a locally homogeneous mesoscopic network of biophysical neurons. Figures 2(d) and 2(e) and Figure 3(a) demonstrate the validity of the stepwise QIF approximation of the original dynamics for different values of $[K^+]_{bath}$ in terms of the simulation of the corresponding dynamics. These figures show that approximating the stepwise QIF captures the behavior of the original 4-dimensional dynamics for the entire biophysical range of $[K^+]_{bath}$. Figure 3(b) illustrates the method for averaging the variable in a 3-dimensional phase space portrait and demonstrate that averaging the variable n (5) and the subsequent stepwise QIF approximation ((10) with no coupling or $J = 0$) still preserve the slow dynamics is shown with 3-dimensional phase space portraits of each of the neurons for $[K^+]_{bath} = 11.5$. In Figure 2(f) the frequencies of these three dynamics are compared for entire range of $[K^+]_{bath}$ to demonstrate that, though there is a small frequency mismatch between these approximations, the overall stepwise QIF approximation captured the slow dynamic behavior of the original complex biophysical process described in (1) qualitatively as well as quantitatively. These allowed us to apply a Lorentzian distribution for the membrane potential and to develop the mean field approximation of a heterogeneous network of biophysical neurons driven by ion exchange dynamics coupled all-to-all via conductance-based coupling (8).

When $\Delta[K^+]_i$ is non-autonomous, the mean field model captures the exact frequency of the oscillation as it is analytically derived by substituting the LA into the continuity equation (12). This is demonstrated in Figure 4(a) for

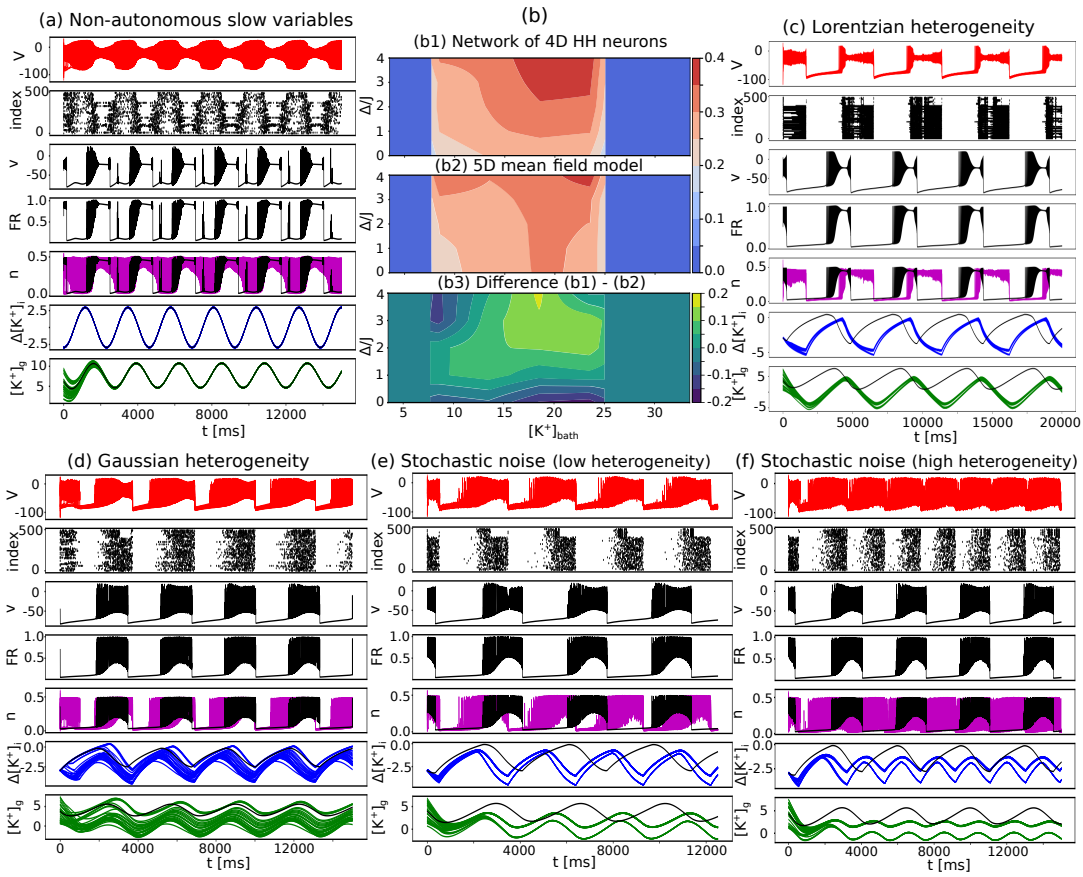

FIGURE 4 Simulations of networks of neurons with the mean field model: V [mV] for the network nodes in the first row (in red); scatter of the firing neurons in the second row; v [mV] for the mean field in the third row (in black); firing rate of the mean field model in the fourth row; n in the fifth row: network nodes in magenta and mean field in black; $\Delta[K^+]_i$ $[mol\backslash m^3]$ in the sixth row: network nodes in blue and mean field in black, and $[K]_g$ $[mol\backslash m^3]$ in the seventh row: network nodes in green and mean field in black, for $[K^+]_{bath} = 12.5$, $J = 4$: (a) Non-autonomous $\Delta[K^+]_i$ for $\frac{\Delta}{J} = 3.0$, with $\Delta[K^+]_i$ as in 26; (c) Lorentzian distribution of heterogeneity η for $\frac{\Delta}{J} = 1.0$; (d) Gaussian distribution of heterogeneity η for $\frac{\Delta}{J} = 4.0$, with stochastic white noise η; (e) $\frac{\Delta}{J} = 2.0$ and (f) $\frac{\Delta}{J} = 3.0$. (b) Frequencies (represented by the color code) of the network of coupled HH neurons as a function of $[K^+]_{bath}$ and relative half-width of heterogeneity $\frac{\Delta}{J}$ in the first row (b1), frequencies (represented by the color code) of the mean field model as a function of $[K^+]_{bath}$ and relative half-width of heterogeneity $\frac{\Delta}{J}$ in the second row (b2), difference between frequencies (represented by the color code) from the network of coupled HH neurons and 5D-mean field model in the third row: for (b3) $J = 4$.

a non-autonomous $\Delta[K^+]_i$ taken as a sinusoidal function. When $\Delta[K^+]_i$ is autonomous (function of state variables only), the mean field model is a mean field approximation, which encounters a frequency mismatch with the locally homogeneous mesoscopic network of biophysical neurons described in (1). Figure 4(c) illustrates the validity of the mean field approximation by a simulated plot from the network of biophysical neurons and the plot of the mean field approximation described in (26). The frequencies of the mean field model and the network of biophysical neurons

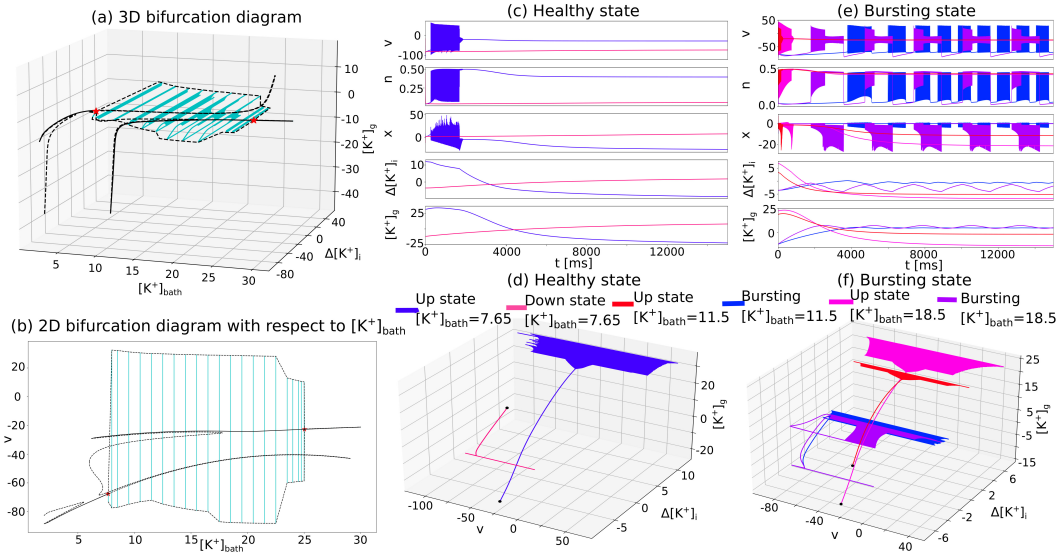

FIGURE 5 Bifurcation diagram of the mean field model: (a) v [mV] and $\Delta[K^+]_i$ $[mol\backslash m^3]$ are represented against $[K^+]_{bath}$ $[mol\backslash m^3]$, (b) v [mV] is represented against $[K^+]_{bath}$ $[mol\backslash m^3]$, the stable fixed points are shown by black lines whereas the unstable fixed points are represented by dotted lines. The maximum and minimum values of the limit cycle are shown by black dotted lines in between the two bifurcation values are shown by red marks. Multistability in the mean field model at $[K^+]_{bath} = 7.65$ (healthy regime) :(c) time series for healthy state ($[K^+]_{bath} = 7.65$) demonstrating the up and down states, up state in blue and down state in red. (d) Three-dimensional phase space in $v, \Delta[K^+]_i$, and $[K]_g$ dimensions for the up and down states: the black marks denote the fixed points in the up and down state. Multistability in the mean field model at $[K^+]_{bath} = 11.5$ and 18.5 (bursting regime): (e) time series for the up and down states: epileptic state in violet, bursting in blue, up states in pink, and red for different values of $[K^+]_{bath}$. (f) Three-dimensional phase space in $v, \Delta[K^+]_i$, and $[K]_g$ dimensions for the up and down states (bursting): the black marks denote the fixed points up states, while the blue and violet phase space trajectories shows the bursting, and epileptic state.

again encounter a slight mismatch, which is illustrated in Figure 4(b) for different values of relative heterogeneity Δ/J. The frequency of oscillation of the network of neurons, the mean field approximation, and their relative differences are represented in Figures 4(b1), 4(b2), 4(b3), respectively, with respect to $[K^+]_{bath}$ and relative heterogeneity Δ/J. This provides evidence that the mean field approximation can capture the network behavior of the large network of neurons quite efficiently in that the relative difference between the frequency of the network of neurons and the mean field approximation is less than 10% for almost the entire regime of relative heterogeneity and $[K^+]_{bath}$.

The simulation of the mean-field model along with the network of single neurons demonstrates that the mean-field approximation is quite robust in terms of the distribution of heterogeneity, as illustrated in Figure 4(d), with a Gaussian distribution of heterogeneity rather than the LA. Moreover, the simulations of a network of single neurons with stochastic white noise reveal that the mean-field model (deterministic) was in agreement with and approximately matched the network of stochastic single neurons for the small variances associated with white noise Figure 4(e), but as the variance increased, the agreement was reduced and eventually for higher variances the similarity was destroyed as the network simulations of stochastic neurons became more and more noisy (Figure 4(f)).

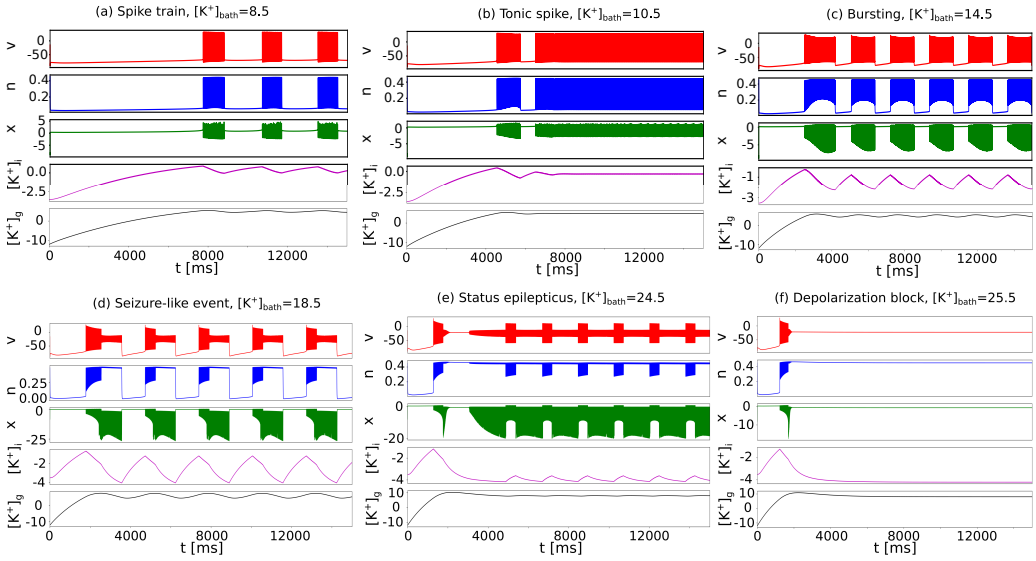

FIGURE 6 Qualitative mode of behavior of the mean field model: time series v [mV] (in red), n (in blue), $\Delta[K^+]_i$ $[mol\backslash m^3]$ (in green), and $[K]_g$ $[mol\backslash m^3]$ (in black) are demonstrated for the following patterns of activity: (a) Spike train at $[K^+]_{bath} = 8.5$, (b) Tonic spiking (TS) at $[K^+]_{bath} = 10.5$, (c) Bursting at $[K^+]_{bath} = 14.5$, (d) Seizure-like event (SLE) at $[K^+]_{bath} = 18.5$, (e) Status epilepticus (SE)-like event at $[K^+]_{bath} = 24.5$, (f) Depolarization block (DB) at $[K^+]_{bath} = 25.5$.

The simulation of the mean-fields dynamics reveals that $[K^+]_{bath}$ serves as a bifurcation parameter of the dynamics. Scanning through its values in the biophysical range changes the behavior of the dynamics from a stable fixed point to an oscillatory limit cycle type of behavior and back to a stable fixed point. To carry out the bifurcation analysis, numerical continuation was applied, and we found that a Hopf bifurcation exists at $[K^+]_{bath} = 7.68$ and a reverse Hopf bifurcation could be found at $[K^+]_{bath} = 25.02$. In between these two values of $[K^+]_{bath}$, the dynamics manifests an oscillatory limit cycle behavior, whereas outside of this range the dynamics of the system shows a stable fixed-point behavior.

Figure 5 presents the 3-dimensional bifurcation diagram (Figure 5(a)) in v and $\Delta[K^+]_i$ with respect to $[K^+]_{bath}$, and the 2-dimensional projections (Figure 5(b)) in the v dimension for the mean-fields model (26), indicating the Hopf bifurcation. However, multistability behavior was found in this model for $[K^+]_{bath} > 5.971$. The existence of multistability in the mean field dynamics is demonstrated in Figure 5. Figure 5(c), and Figure 5(e) illustrates the time series of the dynamics for healthy ($[K^+]_{bath} = 7.65$), and bursting ($[K^+]_{bath} = 11.5, 18.5$) states respectively. whereas Figure 5(d), and Figure 5(f) represent the phase space trajectories for corresponding healthy, and bursting states. Together, they indicate the up state, down state, and epileptic state for different values of $[K^+]_{bath}$. When $[K^+]_{bath}$ is smaller than the Hopf bifurcation, the downstate is found to be a stable fixed-point, which destabilizes into spiking, and bursting behaviors and gradually into epileptic bursts at the bifurcation. On the other hand, the upstate emerges at $[K^+]_{bath} = 5.971$, which is a stable fixed point of the five-dimensional system (25, and 26). However, if the fast subsystem is decoupled and the slow variables are considered to be parameters, the fast subsystem in the upstate undergoes bifurcation, demonstrating a limit cycle, a stable spiral, and a stable fixed point as the value of the slow variable decreases.

The model can also demonstrate different neural activities, as demonstrated in Figure 6. For different regimes of $[K^+]_{bath}$ the mean-field model is capable of producing a large set of brain activities, such as a spike train (Figure 6(a)), tonic spiking (Figure 6(b)), bursting (Figure 6(c)), a seizure-like event (Figure 6(d)), a status epilepticus (SE)-like event (Figure 6(e)), and a polarization block (Figure 6(f)).

Figure 7 represents the effect of a external stimulus current (homogeneous for each network node) on the network of neurons in fixed point regime (healthy regime) at $[K^+]_{bath} = 6.75$ and the network behavior is compared with the mean field model for the same external stimulus current. For better understanding V for some representative network nodes are also presented by sorting the network nodes according to the heterogeneous component η. It is observed that due to the external stimulus the electrical behavior of the neuronal network could switch between up and down states and could emit transient bursts even in the healthy regime. These results are in agreement with experimental results of brain stimulation. Emission of transient bursts are shown for external stimulus current with square wave type external current (Figure 7(a)) and sinusoidal type external current (Figure 7(b)).

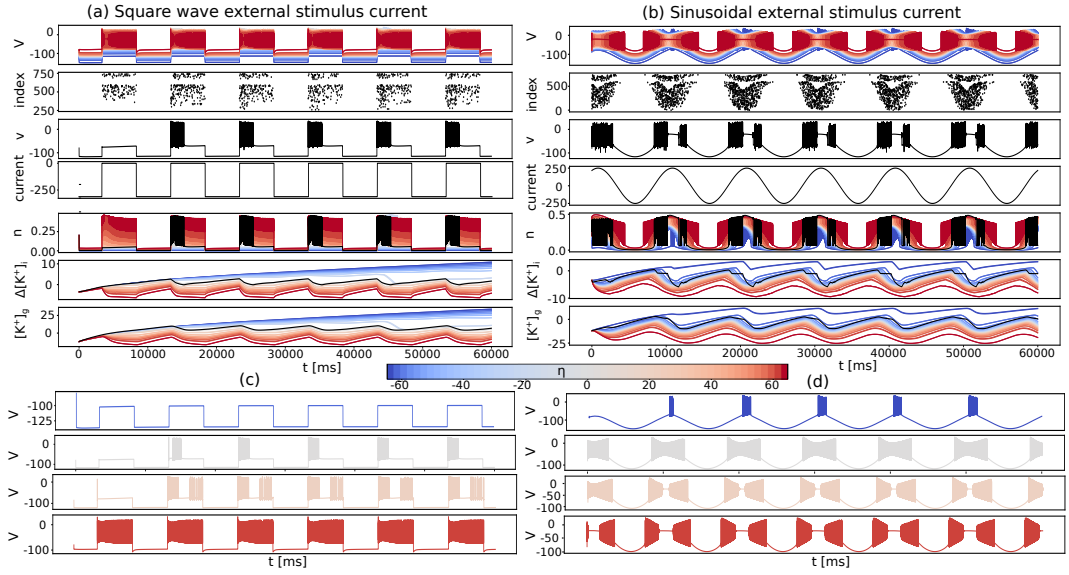

FIGURE 7 Transition between up and down states with external stimulus current in fixed point (healthy) regime $[K^+]_{bath} = 6.75\ [mol\backslash m^3]$. Simulations of networks of neurons with the mean field model: V [mV] for the network nodes in the first row; scatter of the firing neurons in the second row; v [mV] for the mean field in the third row; the external input current [mA] (homogeneous for each node and the same external current is added to the mean field model) in the fourth row; n in the fifth row; $\Delta[K^+]_i\ [mol\backslash m^3]$ in the sixth row, and $[K]_g\ [mol\backslash m^3]$ in the seventh row. The color of the variables in the network of neuron are sorted according to the heterogeneous component η (shown in the color bar) and variables from the mean field model are plotted in black.V [mV] from some representative network nodes are plotted in last four rows. Effect of addition of an external stimulus current is shown for (a)square wave type external current, (b) sinusoidal type external current

5 | CONCLUSION

In this study we developed a biophysically inspired mean field model for an all-to-all connected, locally homogeneous mesoscopic network of Hodgkin–Huxley type neurons. The Lorentzian ansatz makes the mean-field approximation to be analytically tractable, and from the simulation of a network of such neurons it is evident that the mean field model captures the dynamic behavior of the network, while being quite robust for different distributions of heterogeneity. This model relates the mechanism of the biophysical activity of ion exchange and ion channels to the phenomenology of the whole brain dynamics. Also, it demonstrates that the coexistence of resting state brain dynamics and epileptic seizures depends on different states of biophysical quantities and parameters. It is observed that even within the healthy regime different kind of stimulus current, which could be external stimuli or input from some other brain regions could generate transient spiking and bursting activity in different brain regions. Intracellular and extracellular potassium concentrations act as an adaptation (a biophysical regulation that changes the electrical activity of neurons acting on a relatively slow time scale) and relate the slow scale biophysical mechanism in the brain to the fast scale mean field activity of the membrane potential. The model demonstrates different neural activities, such as the existence of up states and down states during the healthy parametric regimes. Increasing the excitability on the other hand leads to appearance of spike trains, tonic spiking, bursting, seizure-like events, status epilepticus -like events, and depolarization block. Our mean-field derivation aggregates a large group of brain behaviors into a single neural mass model, with direct correspondence to biologically relevant parameters. This paves the road for brain network models with bottom-up regional heterogeneity that stems from the structural data features.

references

[1] Deco G, Jirsa VK, McIntosh AR. Emerging concepts for the dynamical organization of resting-state activity in the brain. Nature Reviews Neuroscience 2011;12(1):43–56.

[2] Deco G, Jirsa VK, Robinson PA, Breakspear M, Friston K. The dynamic brain: from spiking neurons to neural masses and cortical fields. PLoS computational biology 2008;4(8):e1000092.

[3] Deco G, Jirsa VK. Ongoing cortical activity at rest: criticality, multistability, and ghost attractors. Journal of Neuroscience 2012;32(10):3366–3375.

[4] Petkoski S, Jirsa VK. Transmission time delays organize the brain network synchronization. Philosophical Transactions of the Royal Society A: Mathematical, Physical and Engineering Sciences 2019;377(2153):20180132. https://royalsocietypublishing.org/doi/10.1098/rsta.2018.0132.

[5] Sanz-Leon P, Knock SA, Spiegler A, Jirsa VK. Mathematical framework for large-scale brain network modeling in The Virtual Brain. Neuroimage 2015;111:385–430.

[6] Wilson HR, Cowan JD. Excitatory and inhibitory interactions in localized populations of model neurons. Biophysical journal 1972;12(1):1–24.

[7] David O, Friston KJ. A neural mass model for MEG/EEG:: coupling and neuronal dynamics. NeuroImage 2003;20(3):1743–1755.

[8] Moran RJ, Kiebel SJ, Stephan KE, Reilly R, Daunizeau J, Friston KJ. A neural mass model of spectral responses in electrophysiology. NeuroImage 2007;37(3):706–720.

[9] Wong KF, Wang XJ. A recurrent network mechanism of time integration in perceptual decisions. Journal of Neuroscience 2006;26(4):1314–1328. http://www.jneurosci.org/cgi/doi/10.1523/JNEUROSCI.3733-05.2006.

[10] Melozzi F, Bergmann E, Harris JA, Kahn I, Jirsa V, Bernard C. Individual structural features constrain the mouse functional connectome. Proceedings of the National Academy of Sciences of the United States of America 2019;116(52):26961–26969.

[11] Courtiol J, Guye M, Bartolomei F, Petkoski S, Jirsa VK. Dynamical mechanisms of interictal resting-state functional connectivity in epilepsy. Journal of Neuroscience 2020;40(29):5572–5588.

[12] Proix T, Bartolomei F, Guye M, Jirsa VK. Individual brain structure and modelling predict seizure propagation. Brain 2017;140(3):641–654. https://academic.oup.com/brain/article-lookup/doi/10.1093/brain/awx004%0Ahttp://www.ncbi.nlm.nih.gov/pubmed/28364550.

[13] Jirsa VK, Stacey WC, Quilichini PP, Ivanov AI, Bernard C. On the nature of seizure dynamics. Brain 2014;137(8):2210–2230.

[14] The Virtual Epileptic Patient: Individualized whole-brain models of epilepsy spread. NeuroImage 2017;145:377–388. http://dx.doi.org/10.1016/j.neuroimage.2016.04.049.

[15] Deco G, Kringelbach ML, Arnatkeviciute A, Oldham S, Sabaroedin K, Rogasch NC, et al. Dynamical consequences of regional heterogeneity in the brain's transcriptional landscape. Science Advances 2021;7(29).

[16] Amunts K, Mohlberg H, Bludau S, Zilles K. Julich-Brain: A 3D probabilistic atlas of the human brain's cytoarchitecture. Science 2020;369(6506):988–992.

[17] Hodgkin AL, Huxley AF. A quantitative description of membrane current and its application to conduction and excitation in nerve. The Journal of physiology 1952;117(4):500–544.

[18] Bazhenov M, Timofeev I, Steriade M, Sejnowski TJ. Potassium model for slow (2-3 Hz) in vivo neocortical paroxysmal oscillations. Journal of neurophysiology 2004;92(2):1116–1132.

[19] Park EH, Durand DM. Role of potassium lateral diffusion in non-synaptic epilepsy: a computational study. Journal of theoretical biology 2006;238(3):666–682.

[20] Fröhlich F, Timofeev I, Sejnowski TJ, Bazhenov M. Extracellular potassium dynamics and epileptogenesis. In: Computational neuroscience in epilepsy Elsevier; 2008.p. 419–439.

[21] Cressman JR, Ullah G, Ziburkus J, Schiff SJ, Barreto E. The influence of sodium and potassium dynamics on excitability, seizures, and the stability of persistent states: I. Single neuron dynamics. Journal of computational neuroscience 2009;26(2):159–170.

[22] Amzica F, Massimini M, Manfridi A. Spatial buffering during slow and paroxysmal sleep oscillations in cortical networks of glial cells in vivo. Journal of Neuroscience 2002;22(3):1042–1053.

[23] Ransom CB, Ransom BR, Sontheimer H. Activity-dependent extracellular K+ accumulation in rat optic nerve: the role of glial and axonal Na+ pumps. The Journal of physiology 2000;522(3):427–442.

[24] Izhikevich EM, Edelman GM. Large-scale model of mammalian thalamocortical systems. Proceedings of the national academy of sciences 2008;105(9):3593–3598.

[25] Montbrió E, Pazó D, Roxin A. Macroscopic description for networks of spiking neurons. Physical Review X 2015;5(2):021028.

[26] Montbrió E, Pazó D. Exact mean-field theory explains the dual role of electrical synapses in collective synchronization. Physical Review Letters 2020;125(24):248101.

[27] Shriki O, Hansel D, Sompolinsky H. Rate models for conductance-based cortical neuronal networks. Neural computation 2003;15(8):1809–1841.

[28] Roxin A, Brunel N, Hansel D. Role of delays in shaping spatiotemporal dynamics of neuronal activity in large networks. Physical review letters 2005;94(23):238103.

[29] Luke TB, Barreto E, So P. Complete classification of the macroscopic behavior of a heterogeneous network of theta neurons. Neural computation 2013;25(12):3207–3234.

[30] Proix T, Bartolomei F, Chauvel P, Bernard C, Jirsa VK. Permittivity coupling across brain regions determines seizure recruitment in partial epilepsy. Journal of Neuroscience 2014;34(45):15009–15021.

[31] Wendling F, Benquet P, Bartolomei F, Jirsa V. Computational models of epileptiform activity. Journal of neuroscience methods 2016;260:233–251.

[32] Ashwin P, Coombes S, Nicks R. Mathematical frameworks for oscillatory network dynamics in neuroscience. The Journal of Mathematical Neuroscience 2016;6(1):1–92.

[33] Devalle F, Montbrió E, Pazó D. Dynamics of a large system of spiking neurons with synaptic delay. Physical Review E 2018;98(4):042214.

[34] Spiegler A, Knösche TR, Schwab K, Haueisen J, Atay FM. Modeling brain resonance phenomena using a neural mass model. PLoS computational biology 2011;7(12):e1002298.

[35] Touboul J, Wendling F, Chauvel P, Faugeras O. Neural mass activity, bifurcations, and epilepsy. Neural computation 2011;23(12):3232–3286.

[36] Baladron J, Fasoli D, Faugeras O, Touboul J. Mean-field description and propagation of chaos in networks of Hodgkin-Huxley and FitzHugh-Nagumo neurons. The Journal of Mathematical Neuroscience 2012;2(1):1–50.

[37] Nevado-Holgado AJ, Marten F, Richardson MP, Terry JR. Characterising the dynamics of EEG waveforms as the path through parameter space of a neural mass model: application to epilepsy seizure evolution. Neuroimage 2012;59(3):2374–2392.

[38] Hocepied G, Legros B, Van Bogaert P, Grenez F, Nonclercq A. Early detection of epileptic seizures based on parameter identification of neural mass model. Computers in biology and medicine 2013;43(11):1773–1782.

[39] El Houssaini K, Ivanov AI, Bernard C, Jirsa VK. Seizures, refractory status epilepticus, and depolarization block as endogenous brain activities. Physical Review E 2015;91(1):010701.

[40] Wang J, Niebur E, Hu J, Li X. Suppressing epileptic activity in a neural mass model using a closed-loop proportional-integral controller. Scientific reports 2016;6(1):1–12.

[41] Laing CR. Phase oscillator network models of brain dynamics. Computational models of brain and behavior 2017;505:517.

[42] Byrne A, Brookes MJ, Coombes S. A mean field model for movement induced changes in the beta rhythm. Journal of computational neuroscience 2017;43(2):143–158.

[43] Bandyopadhyay A, Kar S. Impact of network structure on synchronization of Hindmarsh–Rose neurons coupled in structured network. Applied Mathematics and Computation 2018;333:194–212.

[44] Ullah G, Cressman Jr JR, Barreto E, Schiff SJ. The influence of sodium and potassium dynamics on excitability, seizures, and the stability of persistent states: II. Network and glial dynamics. Journal of computational neuroscience 2009;26(2):171–183.

[45] Depannemaecker D, Ivanov A, Lillo D, Spek L, Bernard C, Jirsa V. A unified physiological framework of transitions between seizures, sustained ictal activity, and depolarization block at the single neuron level. BioRxiv 2021;p. 2020–10.

[46] Destexhe A, Mainen ZF, Sejnowski TJ. An efficient method for computing synaptic conductances based on a kinetic model of receptor binding. Neural computation 1994;6(1):14–18.

[47] Baroni F, Burkitt AN, Grayden DB. Interplay of intrinsic and synaptic conductances in the generation of high-frequency oscillations in interneuronal networks with irregular spiking. PLoS Computational Biology 2014;10(5):e1003574.

[48] Kuramoto Y. Collective synchronization of pulse-coupled oscillators and excitable units. Physica D: Nonlinear Phenomena 1991;50(1):15–30.

[49] Petkoski S, Stefanovska A. Kuramoto model with time-varying parameters. Physical Review E 2012;86(4):046212.